

A 70-year record reveals the poleward shift of tropical cyclone tracks in the east China coastal ocean is twice that of landward shift

Xu, Chaoran; Yang, Yang; Jia, Jianjun; Bricker, Jeremy D.; Wang, Ya Ping

DOI

[10.1016/j.gloplacha.2024.104566](https://doi.org/10.1016/j.gloplacha.2024.104566)

Publication date

2024

Document Version

Final published version

Published in

Global and Planetary Change

Citation (APA)

Xu, C., Yang, Y., Jia, J., Bricker, J. D., & Wang, Y. P. (2024). A 70-year record reveals the poleward shift of tropical cyclone tracks in the east China coastal ocean is twice that of landward shift. *Global and Planetary Change*, 242, Article 104566. <https://doi.org/10.1016/j.gloplacha.2024.104566>

Important note

To cite this publication, please use the final published version (if applicable). Please check the document version above.

Copyright

Other than for strictly personal use, it is not permitted to download, forward or distribute the text or part of it, without the consent of the author(s) and/or copyright holder(s), unless the work is under an open content license such as Creative Commons.

Takedown policy

Please contact us and provide details if you believe this document breaches copyrights. We will remove access to the work immediately and investigate your claim.

Green Open Access added to TU Delft Institutional Repository

'You share, we take care!' - Taverne project

<https://www.openaccess.nl/en/you-share-we-take-care>

Otherwise as indicated in the copyright section: the publisher is the copyright holder of this work and the author uses the Dutch legislation to make this work public.



A 70-year record reveals the poleward shift of tropical cyclone tracks in the east China coastal ocean is twice that of landward shift

Chaoran Xu^{a,b,c}, Yang Yang^d, Jianjun Jia^{b,*}, Jeremy D. Bricker^{c,e,**}, Ya Ping Wang^b

^a National Engineering Research Center of Port Hydraulic Construction Technology, Tianjin Research Institute for Water Transport Engineering, M.O.T., Tianjin 300456, China

^b State Key Laboratory of Estuarine and Coastal Research, School of Marine Sciences, East China Normal University, Shanghai 200241, China

^c Department of Civil and Environmental Engineering, University of Michigan, Ann Arbor 48109, USA

^d School of Marine Science and Engineering, Nanjing Normal University, Nanjing 210046, China

^e Faculty of Civil Engineering & Geosciences, Delft University of Technology, Delft 2628CN, Netherlands

ARTICLE INFO

Editor: Dr Storelvmo Trude

Keywords:

K-means clustering
Tropical cyclone track
Poleward
Landward
East China coastal ocean

ABSTRACT

Analyzing the spatial-temporal changes in tropical cyclone (TC) tracks in the east China coastal ocean (ECCO) to quantify the magnitude of poleward and landward migration of TCs is of significant importance for coastal disaster mitigation and planning due to its susceptibility to the impacts of TCs. In this study, the TCs that affected the ECCO from 1949 to 2022 are classified into three typical types of tracks using the k-means clustering method, mass moments, and track interpolation based on TC location, shape, and intensity information. Type 1 is a northwestward track, Type 2 is a northwest to northeast-turning track, and Type 3 is a northwest to northeast-turning offshore track. Type 1 tracks mainly make landfall in southern China, while Type 2 predominantly makes landfall in eastern China. Moreover, the proportion of Type 1 decreases while their landfall percentage increases over time, and the proportion of Type 2 tracks is increasing. The probability of TC effects on the eastern and northern parts of the ECCO is increasing, and the boundary where the TC center reaches after landfall is shifting landward. During the period from 1994 to 2022, there has been a significant migration in TC tracks, with the mean centroid of the TCs affecting the ECCO shifting westward by 0.66° in longitude and northward by 1.26° in latitude, which means the magnitude of the poleward shift is about twice that of the landward shift. This migration appears to have been pre-conditioned by a combined influence of a weakening westward steering flow, reduced vertical wind shear, and warmer sea surface temperature. Our findings provide valuable insights into the longitudinal and latitudinal migration of TC tracks and have important implications for disaster prevention, mitigation planning, and the adjustment of crucial coastal protection zones in the ECCO and similar regions around the globe.

1. Introduction

Tropical cyclones (TCs) are highly destructive weather systems accompanied by gale-force winds, heavy rainfall, and storm surges (Muis et al., 2016). Over the past 50 years, 1942 disasters worldwide have been attributed to TCs, resulting in 779,324 deaths and US\$140.76 billion in damages (Bangladesh, 2020). The Western North Pacific (WNP) is known for its high TC activity, which poses significant risks to life and property in East Asia. Approximately one-third of these TCs make landfall or affect China, mainly in the East China Sea and the South

China Sea, with fewer occurrences in the Bohai Sea and the North Yellow Sea (Kamahori et al., 2006; Wu et al., 2006; Wang et al., 2021). In China, particularly in the economically developed and densely populated 14 eastern coastal provinces, storm surges account for the highest percentage of marine disaster losses. Despite a decreasing trend in the number of TCs generated in the WNP in recent decades (Qian et al., 2022), there has been a poleward shift in the average latitude where TCs reach their peak intensity in this region (Kossin et al., 2014; Kossin et al., 2016). Additionally, TC tracks have shifted poleward as well (Yumoto et al., 2003; Zhao et al., 2013; Ming et al., 2021) and the landfall

* Corresponding author at: State Key Laboratory of Estuarine and Coastal Research, School of Marine Sciences, East China Normal University, Shanghai 200241, China.

** Corresponding author at: Department of Civil and Environmental Engineering, University of Michigan, Ann Arbor 48109, USA.

E-mail addresses: jjia@sklec.ecnu.edu.cn (J. Jia), jeremydb@umich.edu (J.D. Bricker).

<https://doi.org/10.1016/j.gloplacha.2024.104566>

Received 6 December 2023; Received in revised form 26 August 2024; Accepted 3 September 2024

Available online 5 September 2024

0921-8181/© 2024 Elsevier B.V. All rights are reserved, including those for text and data mining, AI training, and similar technologies.

locations of TCs are mainly determined by their track (Liu et al., 2001). Meanwhile, the strong winds and waves associated with TCs passing over the sea surface can substantially increase current velocity and bed shear stress. This effect leads to sediment resuspension (Hawkes and Horton, 2012) and alters the transport patterns of seafloor sediments (Schuerch et al., 2014). Therefore, analyzing the changes in TC tracks not only improves the ability to respond to risks but also supports the study of sediment transport patterns during TCs.

TC generation and development are closely related to local thermodynamic and dynamical conditions, especially the changes in steering flow, vertical wind shear stress (VWS), and sea surface temperature (SST) (Mei and Xie, 2016; Camargo and Wing, 2021). The steering flow can lead the movement of TCs. For example, the migration of TCs towards coasts maybe caused by the westward trend of steering flow in the WNP (Wang and Toumi, 2021). Weak VWS is essential for the maintenance and development of TCs (Emanuel, 1999; Ting et al., 2019), and may also contribute to geographical shifts of TC locations combined with the change of steering flow (Kossin et al., 2014; Wang and Toumi, 2021). The influence of warming SST leads to the meridional expansion of the tropical region and energizes the development of TCs (Mei et al., 2015; Sharmila and Walsh, 2018). This results in the northward movement of TCs, potentially increasing the risk of TC-related hazards in higher-latitude regions. According to the China Marine Disaster Bulletin 1989–2020 (<http://www.mnr.gov.cn/sj/sjfw/hy/gb/gg/zghyzhgb/>), direct economic losses in the Yellow Sea and the East China Sea (the east China coast ocean, referred to as “ECCO” hereafter, Fig. 1a), including several high-latitude coastal provinces of China, are high and volatile. A comprehensive assessment of future TC risk, especially on a regional scale, requires an in-depth understanding of the spatial variability of TC tracks in the ECCO.

Most studies analyzing the spatial variability of TC tracks affecting

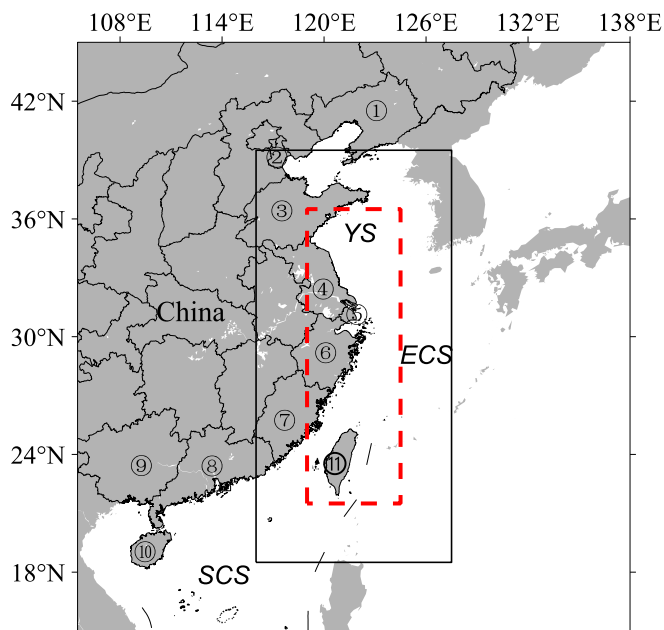


Fig. 1. Study area. The red dashed box is the study area, the black box is the range of TC centers that may affect the study area (hereinafter referred to as “affected area”), and circled numbers are the coastal provinces of China’s mainland and Taiwan region: ①Liaoning, ②Tianjin, ③Shandong, ④Jiangsu, ⑤Shanghai, ⑥Zhejiang, ⑦Fujian, ⑧Guangdong, ⑨Guangxi, ⑩Hainan, and ⑪ Taiwan; YS is the Yellow Sea, ECS is the East China Sea, SCS is the South China Sea. (For interpretation of the references to colour in this figure legend, the reader is referred to the web version of this article.) (For interpretation of the references to colour in this figure legend, the reader is referred to the web version of this article.) (For interpretation of the references to colour in this figure legend, the reader is referred to the web version of this article.)

China focus on the TCs throughout the entire generating region: TC tracks generated in the WNP (Mei and Xie, 2016; Zhao et al., 2020; Meng et al., 2023); TC tracks generated in the South China Sea (Luo et al., 2022; Yin et al., 2023) and other related studies. For example, Zhao et al. (2013) pointed out that in the late 1980s, there was a noticeable northwestward shift in TC tracks across the entire WNP. Additionally, Wang and Toumi (2021) demonstrated a clear trend of onshore development for TCs in the WNP. By selecting representative TCs over the East China marginal sea, Xu et al. (2022) found that TCs show a poleward and landward migration. This provides valuable guidance for analyzing TC tracks that affect China. However, in previous studies, their analysis primarily focuses on all TC tracks within the generating region, with limited research on the regional response in the ECCO caused by changes in TC tracks, and the lack of a systematic analytical methodology for how to select representative TCs that affected specific regions. Xu et al. (2022) employed a TC wind field model to calculate the wind speed distribution of TCs over the ECCO since 1949 and found that TCs affecting this region can be categorized into three historical periods and that the TC activity exhibits both poleward (northward) and landward (westward) shifting trends. This provides a foundation for analyzing the poleward and landward shifts of TC tracks in a specific region. However, Xu et al. (2022) only found vague trends in the poleward and landward migration, and did not reveal the exact extent and magnitude of the poleward and landward migration. Further study to find out the exact extent and magnitude of the poleward and landward migration in the specific region is important for regional disaster prevention planning.

Conducting the classification of TC tracks in this region is a vital method for acquiring TC characteristics and assessing their effect (Shen et al., 2018; Meng et al., 2023; Yin et al., 2023). There are two main methods for TC track classification: the subjective identification method (Colbert and Soden, 2012; Hu et al., 2020) and the clustering analysis method (Nakamura et al., 2009; Meng et al., 2023). The clustering analysis method is more objective and convenient compared to the subjective identification method, as the K-means clustering method can effectively differentiate TCs by taking into account the TC position, track shape, intensity, and other circumstances and is widely used to classify TC tracks in the Indian Ocean (Paliwal and Patwardhan, 2013), Atlantic (Nakamura et al., 2009; Nakamura et al., 2021), and WNP (Meng et al., 2023; Yin et al., 2023). In this study, we build on Xu et al. (2022) to further analyse the temporal and spatial variability of TCs in this region and quantify the exact extent and magnitude of the poleward and landward migration of the TCs affecting the ECCO. The selected TCs affecting the ECCO are first classified using the K-means clustering analysis method based on their positions, shapes, and intensities. Then we use the classified results to analyse the longitudinal and latitudinal response of TC tracks and the landward extent of TC centers after landfall. This analysis allows us to deepen our knowledge of the exact extent and magnitude of the poleward and landward migration of TC tracks over the ECCO during the past 70 years.

2. Materials and methods

2.1. Study area

The ECCO (Fig. 1) is one of the most severely affected by TCs. The densely populated and rapidly growing economy of the ECCO has rendered the region highly susceptible to natural disasters, resulting in significant annual losses attributed to TCs (Wang and Song, 2011; Xu and Huang, 2011). This study concentrates on the ECCO, spanning from 21.5°N to 36.5°N and 119°E to 124.5°E (the area outlined in the red dashed box in Fig. 1), encompassing significant eastern provinces like Shandong, Jiangsu, Shanghai, Zhejiang, and Fujian, which are economically developed and important provinces in eastern China.

2.2. Data source

The TC tracks analyzed in this study were pre-selected from our previous analysis of TCs affecting the ECCO from 1949 to 2022 based on the China Meteorological Administration (CMA) Tropical Cyclone Best Track Dataset (Xu et al., 2022). In the pre-selection process, data of TCs that entered the affected area (indicated by the black solid box in Fig. 1) were analyzed. Using a TC wind field model, wind speed distributions for these TCs across the affected area were calculated. TCs capable of generating wind speeds of 10.8 m/s or faster within the study area (indicated by the red dashed box in Fig. 1) were retained for further analysis and categorized into three historical periods: first period (1949–1967), second period (1968–1993), and third period (1994–2022). For detailed calculations, please refer to Xu et al. (2022). The detailed information for each TC in this study was obtained from the Shanghai Typhoon Institute of the CMA (www.typhoon.org.cn) (Feng et al., 2014; Lu et al., 2021). It contains the time, eye latitude, eye longitude, minimum pressure, and maximum wind speed of the TC over the WNP every 6 h from 1949 to 2022. Monthly averaged mesoscale environmental data (meridional and zonal wind speeds at 200 hPa, 500 hPa, and 850 hPa, and SST) over the period 1949–2022 with a horizontal resolution of $0.25^\circ \times 0.25^\circ$ in the WNP are available from the fifth generation ECMWF atmospheric reanalysis of global climate and weather (ERA5) (Hersbach et al., 2023a, 2023b).

2.3. Clustering methodology

2.3.1. Mass moments

The varying lengths and shapes of TC tracks make it crucial to employ a standardized method for classification. Nakamura et al. (2009) proposed a unified approach utilizing the mass moments method to describe TC tracks consistently. In this method, the mass moments of the open curve defining the entire TC track are utilized to consider both the shape and length of the track comprehensively. This method has been widely adopted by many researchers for analyzing TC tracks (Yu et al., 2016; Nakamura et al., 2017; Wang et al., 2022; Yin et al., 2023). The method is defined and illustrated below.

First, the calculation for the latitude and longitude of the centroid of a TC track are given by Eq. (1) and Eq. (2)

$$\bar{X} = \frac{1}{\sum_{i=1}^n w(i)} \sum_{i=1}^n w(i) x_i, \quad (1)$$

$$\bar{Y} = \frac{1}{\sum_{i=1}^n w(i)} \sum_{i=1}^n w(i) y_i, \quad (2)$$

where \bar{X} and \bar{Y} are the longitude and latitude of the centroid, x_i and y_i are the i -th longitude and latitude of the TC center, n is the number of TC center locations, $w(i)$ is a weight associated with the TC center (in this study, this weight is equal to $\sqrt{v_i}$, this allows the classification of TCs taking into account the intensity information (Nakamura et al., 2009; Yu et al., 2016), where v_i is maximum wind speed of the TC when the center is at location i).

Second, the variance of a TC track can be calculated by the following formula:

$$\text{Var}(x) = \frac{1}{\sum_{i=1}^n w(i)} \sum_{i=1}^n w(i) (x_i - \bar{X})^2, \quad (3)$$

$$\text{Var}(y) = \frac{1}{\sum_{i=1}^n w(i)} \sum_{i=1}^n w(i) (y_i - \bar{Y})^2, \quad (4)$$

$$\text{Var}(xy) = \frac{1}{\sum_{i=1}^n w(i)} \sum_{i=1}^n w(i) (x_i - \bar{X})(y_i - \bar{Y}), \quad (5)$$

where $\text{Var}(x)$, $\text{Var}(y)$, and $\text{Var}(xy)$ respectively represent the variance in the longitudinal, latitudinal, and diagonal directions.

These five values (two centroids and three variances) together form

the summary of the track information that will be used to identify track clusters. The two centroids determine the position of the effective center of gravity of the TC track, whereas the three variances offer an indication of the TC track's shape. The classical covariance measure is often explained as a way to gauge the orientation and length of the principal axes of an ellipse that describes the data's dispersion in a plane.

2.3.2. K-means clustering

In this study, we employ the K-means method with a vector consisting of the five parameters defined in section 2.3.1 (two for latitudinal and longitudinal centroids and three for the variances) for identifying clusters from vector data. The variance components have considerably larger values compared to the centroid components. To ensure that both centroid and variance have equal weight in the clustering analysis, the variables are standardized; each centroid column is then multiplied by 0.5/2, and each variance column by 0.5/3 (Nakamura et al., 2009; Yu et al., 2016). This equalizes the importance of centroids and variances in the clustering process.

The results of the K-means clustering analysis are expressed using the absolute distance between the two TC samples, as shown in Eq. (6):

$$d_{h,l} = \sum_{m=1}^5 |T_{hm} - T_{lm}|, \quad (6)$$

where T_h and T_l represent the serial numbers of TC samples, and m represents the above five indicators. The classification results require the absolute distance between samples of different clusters to be the longest possible, and the distance between samples within a cluster to be the shortest possible.

The K-means cluster analysis package available in Matlab R2022b considers multiple runs with random seeding of clusters. The optimal number of clusters is determined by finding the maximum mean and the minimum number of negative ‘‘Silhouette’’ values. The Silhouette value measures both the cohesion within each cluster and the separation between clusters. For a total of j points, the Silhouette score (S_j) is defined as follows:

$$S_j = \frac{\min(b_j) - a_j}{\max[a_j, \min(b_j)]}, \quad (7)$$

where a_j signifies the mean distance from the j -th point to the other points within its own cluster, and b_j represents the mean distance from the j -th point to points in a different cluster (Kaufman and Rousseeuw, 1990). Silhouette values range from -1 to 1 . Clusters with a high mean silhouette value are cohesive and negative silhouette values are possible misclassified points.

2.3.3. Interpolation of tropical cyclone track

The interpolation of TC track method allows for the transformation of TC tracks with different data lengths into tracks of the same length, this method involves artificial interpolation of each TC track (the initial total number of TC centers is n) into M segments ($M+1$ data points) of equal length while omitting time information (Kim et al., 2011). After clustering analysis, we can calculate the mean track within each cluster by employing this method. This facilitates the comparison of the mean tracks from different clusters, enabling a clearer visualization of the differences in tracks among the various clusters.

For any single TC, the distance between 6-hourly segments of the original best-track data is defined as Eq. (8)

$$\text{dist}_i = \sqrt{(x_{i+1} - x_i)^2 + (y_{i+1} - y_i)^2} \text{ for } i = 1, \dots, n-1, \quad (8)$$

The length of interpolated segments is defined as Eq. (9)

$$\text{edist} = 1 / \left(M \sum_{i=1}^{n-1} \text{dist}_i \right), \quad (9)$$

where M is the number of interpolated segments. The interpolated positions (x_k, y_k) are defined as:

$$x_k = x_1, y_k = y_1 \text{ for } k = 1, \quad (10)$$

$$x_k = x_n, y_k = y_n \text{ for } k = M + 1, \quad (11)$$

$$\begin{cases} x_k = x_l + \frac{(x_{l+1} - x_l)}{\text{dist}_l} \left[(k - 1) \text{edist} - \sum_{i=1}^{l-1} \text{dist}_i \right] \\ y_k = y_l + \frac{(y_{l+1} - y_l)}{\text{dist}_l} \left[(k - 1) \text{edist} - \sum_{i=1}^{l-1} \text{dist}_i \right] \end{cases}, \quad (12)$$

for $k = 2, \dots, M$,

Where l is an integer that satisfies condition (13)

$$\sum_{i=1}^{l-1} \text{dist}_i \leq (j - 1) \times \text{edist} < \sum_{i=1}^l \text{dist}_i \text{ for } k = 2, \dots, M. \quad (13)$$

This procedure can determine new positions along the line connecting the original 6-hourly positions. The interpolated TC track retains the shape, length, and geographical track information covering the TC track data, and is a widely used method (Kim et al., 2011; Zhang et al.,

2015).

3. Results

3.1. Centroids and variances among three periods

We use the mass moments analysis to calculate the mean centroid locations and directional variances of the TC tracks for each of the three historical periods. The TC tracks in the third historical period (1994–2022) exhibit clear separation without overlapping those of the other two periods (1949–1967, 1968–1993), and the variance ellipses emphasize the distinct shape characteristics of each period (Fig. 2). The mean TC track centroid of the first period is positioned furthest south, with a larger variance in longitude compared to latitude with a negative tilt (negative mean variance) as shown in Table 1. The tilt represents the rotation angle of the major axis of the ellipse in the larger direction. The major axis of the variance ellipse indicates the direction and extent of the maximum distribution of track points. Conversely, the minor axis of the variance ellipse reflects the level of concentration in the distribution of tropical cyclone tracks in this direction (Nakamura et al., 2009; Yin et al., 2023). In the second period, the mean centroid of the TC tracks shows little change compared to the first period, with a slight shift towards the northeast. The variance in longitude is larger than in latitude, with a negative tilt. Additionally, the variance ellipse in the second

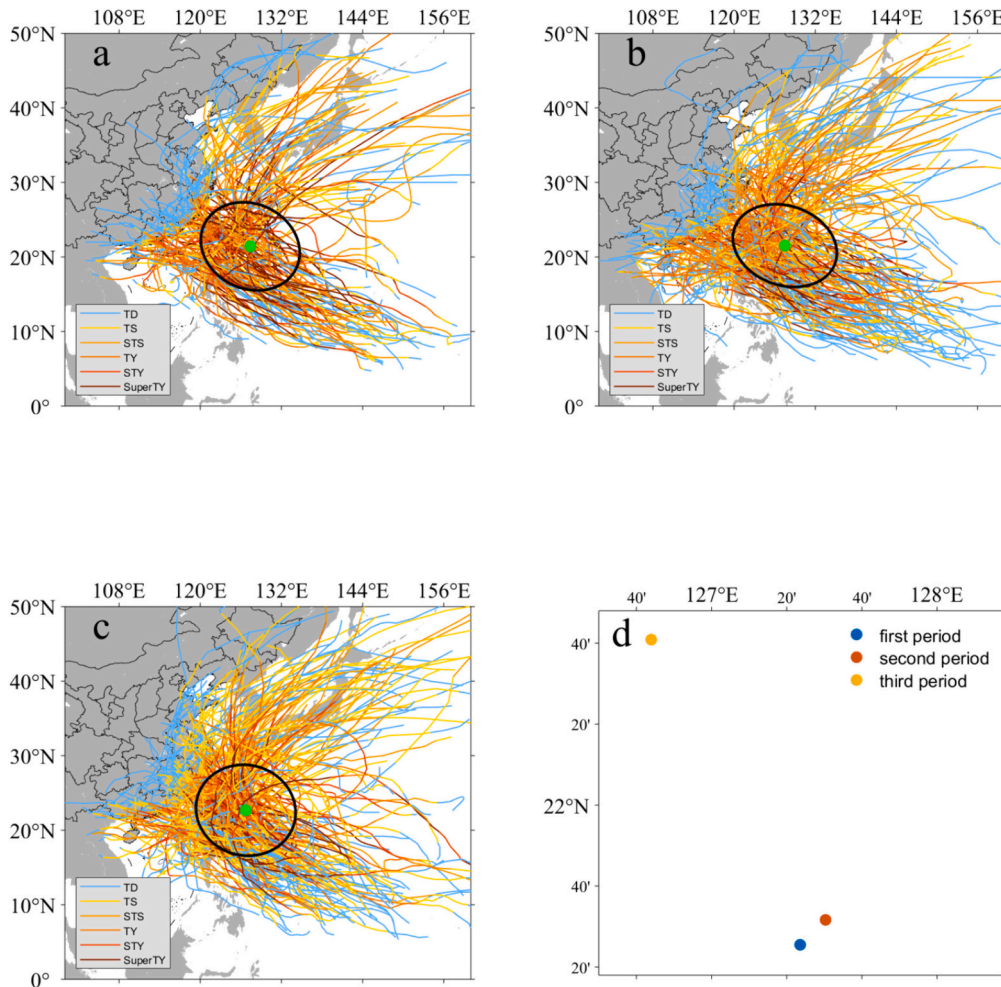


Fig. 2. Mean centroid locations (green dots) and mean variance ellipses (black circles) for each historical TC track period. a is the first period (1949–1967); b is the second period (1968–1993); c is the third period (1994–2022); d is a map showing the three mean centroids together; the colored lines in a–c are individual TC tracks. (For interpretation of the references to colour in this figure legend, the reader is referred to the web version of this article.) (For interpretation of the references to colour in this figure legend, the reader is referred to the web version of this article.)

Table 1
Mean centroid and variance values of the variance ellipse for each period.

Historical Period	Longitude centroid (°E)	Latitude centroid (°N)	Longitudinal Variance (deg ²)	Latitudinal Variance (deg ²)	Diagonal Variance (deg ²)
First(1949–1967)	127.39	21.42	55.36	33.10	−7.48
Second(1968–1993)	127.51	21.53	61.13	28.84	−8.84
Third(1994–2022)	126.73	22.68	54.55	36.98	−2.33

period is similar in shape to that of the first period but with a larger longitudinal variance. For the third period, the mean centroid of TC tracks notably moves northward and westward compared to the first and second period, shifting 1.26° in latitude and 0.66° in longitude. Moreover, its variance ellipse is nearly circular, indicating minimal tilt.

3.2. Characteristics of clusters

3.2.1. Optimal number of clusters

To further analyse the characteristics of TC tracks in each period, clustering analysis methods need to be applied to categorize the tracks for each period. Prior to this, the optimal number of clusters must be determined using the Silhouette score method outlined in Section 2.3.2. This method requires us to set the number of clusters in advance, and select the optimal number of clusters based on the Silhouette score results corresponding to different numbers of clusters. In this study, 2–8 clusters are randomly selected as the initial mean vector of the K-means algorithm. The maximum mean and the minimum number of negative values of S_i are shown in Fig. 3.

In the first period, the maximum mean value of S_i occurs when the number of clusters is 3, and the minimum number of negative values of S_i occurs with 3, 5, 6, or 7 clusters. In the second period, the maximum mean values of S_i occur with 2, 3, or 4 clusters, with the minimum number of negative values of S_i occurring for 3 clusters. In the third period, the maximum mean values of S_i are observed for 3 clusters, and the minimum number of negative values of S_i with greater than 6 clusters. However, even though the minimum number of negative values

of S_i for 3 clusters, doesn't represent the absolute minimum, it is very close to the minimum in the third historical period. It's important to note that a higher number of clusters is not necessarily better, as it can lead to results that are harder to generalize (Zheng et al., 2015; Yu et al., 2016). Therefore, based on this analysis, the optimal number of clusters for this study is 3, which aligns with the classification of TC tracks over the WNP (Zhao et al., 2020; Meng et al., 2023). Therefore, this study categorizes the TC tracks of each period into three clusters, resulting in a total of nine clusters. In the subsequent analysis, the first, second, and third clusters of the first historical period are abbreviated as p1c1, p1c2, and p1c3, respectively. Similarly, for the second period, they are denoted as p2c1, p2c2, and p2c3, and for the third period, as p3c1, p3c2, and p3c3.

3.2.2. Spatial distribution of all TC clusters

K-means clustering analysis also results in the centroid location and directional location of the variance ellipse for each TC cluster in every historical period (Table 2). The centroids of the three clusters in each period exhibit distinct differences, and the shapes of the variance ellipses also vary. Among them, the centroids of p1c1, p2c1, and p3c1 are located in the southwestern-most part of each period. Their longitudinal variances are slightly larger than their latitudinal variances, displaying a negative tilt and forming ellipses expanding in the northwest direction. The centroids of p1c2, p2c2, and p3c2 are situated more towards the northeast compared to p1c1, p2c1, and p3c1. Their longitudinal variances are very close to the latitudinal variances, displaying a very small negative tilt and forming nearly circular. The centroids of p1c3, p2c3, and p3c3 are located in the northeastern-most part of each period. Their longitudinal variances are significantly larger than the latitudinal variances, displaying a strong positive tilt and forming ellipses expanding in the northeast direction.

In order to better visualize the differences among the tracks within each cluster, following the method in section 2.3.3, the lifetime of each TC is divided into an average of 28 time nodes (7 days, which is the mean TC life span based on the analysis of TC life span in section 3.3) arranged chronologically. Subsequently, the time series of TC positions are obtained by averaging the interpolated positions at these nodes. Finally, the TC mean track is derived by averaging the positions of corresponding time nodes among all TC tracks. The mean track for each cluster is represented by the black dots in Fig. 4. From Fig. 4, we can see that p2c1 and p3c1 represent a typical type of TC track moving northwestward and potentially making landfall in China. Although the mean track of p1c1 shows a slight northeastward turn towards the end of its lifetime, this deviation is small. Combined with the characteristics of the variance ellipses, we categorize p1c1, p2c1, and p3c1 as westward TC tracks. Furthermore, these tracks have the shortest track lengths. Moreover, with time, the westward and northward trends of this typical track become increasingly evident. p1c2, p2c2, and p3c2 represent a typical type of TC track characterized by an initial northwest propagation, then turning to the northeast. These TCs develop primarily in the ECCO throughout their lifetime and have slightly longer track lengths compared to the previous typical TC track. Although the mean centroid positions of this track show relatively minor changes over time, the variance ellipses indicate an expanding trend. With time, the range covered by these ellipses increases, potentially affecting more areas in the ECCO. The mean tracks of p1c3, p2c3, and p3c3 are similar to the second cluster mean tracks but are located farther offshore. These mean tracks have the longest track lengths. We define them as northwest to

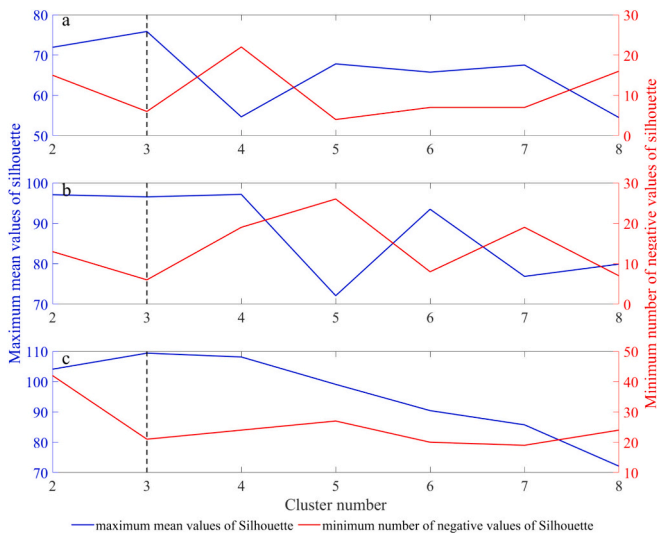


Fig. 3. The result of silhouette analysis in the three historical periods. a is the first period(1949–1967), b is the second period(1968–1993), c is the third period(1994–2022). The blue line is the maximum mean value of S_i , and the red line is the minimum number of negative values of S_i , the black dashed line corresponds to the location where the optimal number of clusters occurs. (For interpretation of the references to colour in this figure legend, the reader is referred to the web version of this article.) (For interpretation of the references to colour in this figure legend, the reader is referred to the web version of this article.) (For interpretation of the references to colour in this figure legend, the reader is referred to the web version of this article.)

Table 2
Mean centroid and variance values of the variance ellipse for each cluster.

Historical Period	Cluster	Longitude centroid (°E)	Latitude centroid (°N)	Longitudinal Variance (deg ²)	Latitudinal Variance (deg ²)	Diagonal Variance (deg ²)
First(1949–1967)	p1c1	125.88	18.56	55.05	19.32	−17.41
	p1c2	129.01	25.51	35.57	53.14	−3.16
	p1c3	135.26	27.00	241.59	56.08	101.98
Second(1968–1993)	p2c1	125.15	18.68	58.66	16.87	−15.14
	p2c2	130.11	25.90	42.18	40.17	−9.71
	p2c3	135.19	25.30	166.09	76.39	46.68
Third(1994–2022)	p3c1	122.79	19.98	37.43	17.07	−10.62
	p3c2	130.59	25.30	59.30	50.74	−5.07
	p3c3	136.02	29.29	232.20	149.44	141.32

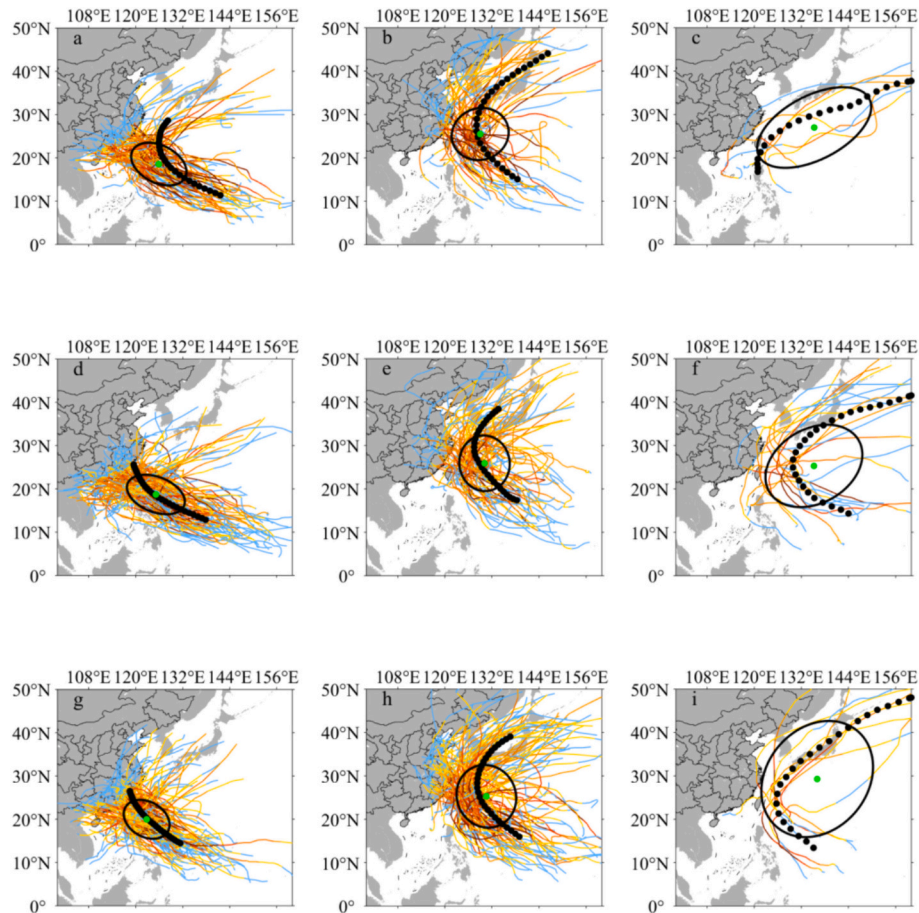


Fig. 4. Mean centroid locations, mean variance ellipses, and mean TC track for each cluster. a-i are p1c1, p1c2, p1c3, p2c1, p2c2, p2c3, p3c1, p3c2, and p3c3, respectively. The red dots are mean centroids locations, the black circles are mean variance ellipses, the black dots are mean TC tracks, and the colored lines in a-i are individual TC tracks. (For interpretation of the references to colour in this figure legend, the reader is referred to the web version of this article.) (For interpretation of the references to colour in this figure legend, the reader is referred to the web version of this article.) (For interpretation of the references to colour in this figure legend, the reader is referred to the web version of this article.)

northeast-turning offshore tracks. Although there are fewer TCs with this typical track, it still tends to move towards the coast and northward. Therefore, we summarize three typical types of TC tracks affecting the ECCO: northwestward (Type 1), northwest to northeast-turning (Type 2), and northwest to northeast-turning offshore (Type 3). This is consistent with the classification results of TC tracks in the entire WNP as presented by Zhao et al. (2020) and Meng et al. (2023).

3.3. Lifespan, Landfall, and Seasonality

The length of TC tracks is generally consistent with their lifespan, which plays a crucial role in determining TC intensity (Camargo et al.,

2007). Most powerful TCs are generated in ocean basins far from coastlines, ensuring they have ample time for full development, and the longer the lifespan, the higher the probability of further development (Li et al., 2010; Song et al., 2018). Fig. 5 illustrates the variations in TC lifespans ranging from 2 to 17 days, with the majority fluctuating between 6 and 12 days. Therefore, in section 3.2.2, we opted for a 28 points/7 days interpolation based on the lifespan of the majority of TCs. This method is commonly used to determine the number of interpolation points when calculating the mean TC track (Nakamura et al., 2009; Shen et al., 2018). We can observe that as TC tracks move farther away from the coastline, the lifespan of TCs gradually increases. Type 3 has the longest mean lifespan, followed by Type 2, and Type 1 has the shortest

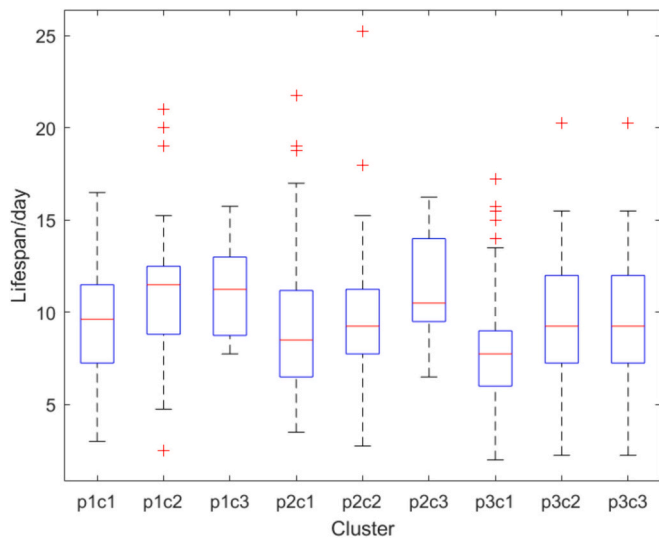


Fig. 5. Box-whisker plot for TC lifespan in each cluster. The red lines represent the medians, the blue boxes represent the 25 %–75 % data intervals, the black dashed lines represent the upper and lower data limits, and the red crosses represent outliers. (For interpretation of the references to colour in this figure legend, the reader is referred to the web version of this article.) (For interpretation of the references to colour in this figure legend, the reader is referred to the web version of this article.) (For interpretation of the references to colour in this figure legend, the reader is referred to the web version of this article.)

mean lifespan. This variation aligns with the lengths of the three typical types mentioned in section 3.2.2. Because type 2 and type 3 move northeastward, they stay longer over the open ocean compared to Type 1. However, Type 1 exhibits more greater intensity in its lifespan compared to the other two typical types. This phenomenon could be attributed to the slower movement of TCs at low latitudes and their faster movement at higher latitudes (Chang and Yu, 2017), therefore, some Type 1 TCs may spend a longer part of their lifespan on a short track at low latitude than on a long high-latitude track. The lifespan of a TC typically influences the size of the variance ellipse; a longer track results in a larger ellipse, unless the TC is exceptionally slow-moving (Nakamura et al., 2009). The variance ellipse in section 3.2.2 also exhibits this variation.

From 1949 to 2022, a total of 590 TCs have affected the ECCO. From Table 3, we can see that Type 1 is the most prevalent in each period, constituting 59.6 %, 60 %, and 52.1 % of TCs, respectively. Type 2 comes next, accounting for 36.4 %, 32.7 %, and 44 % of TCs in each historical period. Type 3 is the least common, making up 4.0 %, 7.3 %, and 3.9 % respectively. Meanwhile, the percentage of Type 2 increases

Table 3

Number of TCs, TC percentage, number of landfalls, and landfall percentage. The TC percentage represents the proportion of each type of TC track to the total number of TC tracks in that specific period. The landfall percentage represents the proportion of each type of TC track to the total number of TC tracks in that specific cluster.

cluster	TC number	TC Percentage (%)	Landfall number	Landfall percentage (%)
p1c1	90	59.6	45	50.0
p1c2	55	36.4	30	54.6
p1c3	6	4.0	2	33.3
p2c1	123	60.0	60	48.8
p2c2	67	32.7	28	41.8
p2c3	15	7.3	2	13.3
p3c1	122	52.1	71	58.2
p3c2	103	44.0	44	42.7
p3c3	9	3.9	3	33.3
total	590	–	285	48.3

between the second and third period, while the percentage of Type 1 decreases. In the second and third periods, the percentage of landfalls for Type 1 is higher than Type 2, while in the first period, the landfall percentages for both types are similar. From Fig. 4, it can be observed that Type 1 is closer to land and tends to move more northwestward, whereas Type 2 is farther from land and moves in a northeastward direction away from the coast. Landfall percentages of both Type 1 and 2 show increase. This analysis of the TC percentage and landfall percentage in each cluster can aid in disaster risk reduction by enhancing our understanding of the relative landfall probability for countries exposed to TCs.

The differences among the nine clusters in the study period should also be taken into account. Fig. 6 illustrates that the primary active period for TCs affecting the ECCO is from April to December. Type 1 has the longest active period, ranging from April to December. Type 2 and Type 3 exhibit relatively smaller fluctuations in their active periods, primarily from May to October. According to the different active months, we can categorize the active periods of the three typical types into three seasons: pre-peak, peak, and post-peak. For Type 1, the three seasons are April to June, July to September, and October to December, respectively. For Type 2, the seasons are May to June, July to September, and October. Due to the smaller number of TCs, Type 3 is categorized into seasons consistent with Type 2 in this study. It can be seen that the most active period for all three typical types is from July to September. Additionally, the pre-peak and post-peak periods for Type 1 are longer compared to the corresponding active periods for the other two types. This could be attributed to the fact that TC generation requires high SST (Emanuel, 1986; Emanuel, 2003). Type 1, being at the lowest latitudes, experiences higher sea surface temperatures in this region, leading to longer active periods. The little high fluctuations in Type 3 may be due to the lower number of TCs of this type.

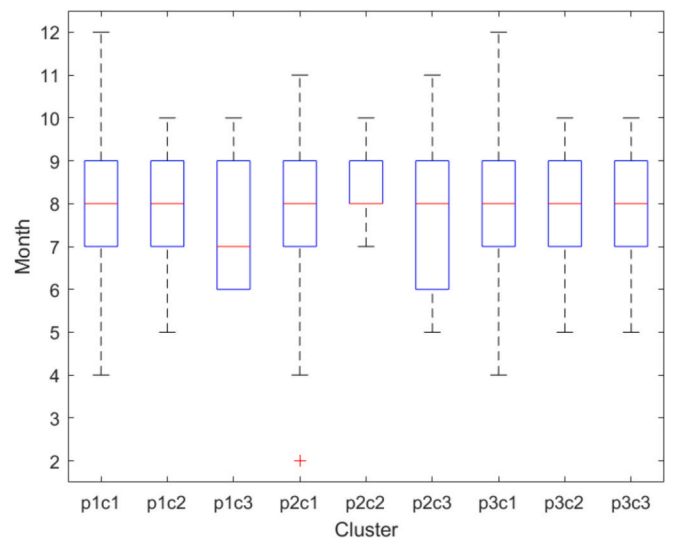


Fig. 6. Box-whisker plot for the month of each TC's lifespan in each cluster. The red lines represent the medians, the blue boxes represent the 25 %–75 % data intervals, the black dashed lines represent the upper and lower data limits, and the red crosses represent the outliers. (For interpretation of the references to colour in this figure legend, the reader is referred to the web version of this article.) (For interpretation of the references to colour in this figure legend, the reader is referred to the web version of this article.) (For interpretation of the references to colour in this figure legend, the reader is referred to the web version of this article.)

4. Discussion

4.1. Longitudinal and latitudinal response of TC tracks

Storm surges, especially when they align with exceptionally high tides and waves, have the potential to cause significant storm surge disasters, posing threats to critical infrastructures such as ports, fisheries, and engineering facilities (Yang et al., 2016). All 11 coastal provinces in mainland China are exposed to varying degrees of these threats. From Section 3.1, the mean centroid position of TCs affecting the ECCO is shifting northward (in the latitudinal direction) and closer to the coast (in the longitudinal direction). Moreover, in Section 3.2.2, both TC tracks of Type 1 and Type 3 exhibit a noticeable northward shift. Although the mean track change for Type 2 is not as pronounced, the variance ellipse of the mean track shows an expansion trend both towards the coast and northward. This phenomenon can also be interpreted as Type 2 tracks fluctuating and expanding northward and closer to the coast.

From the perspective of each TC track's mean centroid relative to its entire track, the centroid is located approximately in the middle portion of the TC track. This area coincides with the region where the TC intensity is strongest (Fig. 2). This is close to the location of a TC's Lifetime Maximum Intensity (LMI). The location of the LMI serves as a crucial indicator for tracking the migration of TCs. The poleward and landward migration of TCs has been widely studied (Kossin et al., 2014; Moon et al., 2015; Feng et al., 2021; Wang and Toumi, 2021; Li et al., 2022; Meng et al., 2023). Therefore, we approximate the change in the mean centroid of TC tracks as the change in the LMI to indicate the migration of TC tracks in the ECCO. The second historical period and the first historical period show minor changes in the mean centroid, while the third historical period experienced a larger change in the mean centroid location. In Section 3.1, it was found that during this period, the mean centroid shifted westward by 0.66° in longitude and northward by 1.26° in latitude. By analyzing TC tracks, we quantified the magnitude of poleward and landward migration of TCs in the 70-year record. This reveals the poleward shift of TC tracks in ECCO is twice the landward shift. This is a quantitative analysis of TC tracks based on the qualitative result of Xu et al. (2022).

To assess the validity of the change of the TC tracks presented in this study, we compare the latitudinal and longitudinal migration rates of TCs affecting the ECCO with TCs generated in the entire WNP. The data collected for previous study spans from 1979 to 2018. Therefore, we perform linear regression on the annual mean longitude and latitude of TC centroids during 1979–2018, deriving their decade migration rates in the ECCO. As shown in Fig. 7, the migration rate of TC tracks in this region is $0.2^\circ/\text{decade}$ in longitude and $0.51^\circ/\text{decade}$ in latitude. As

shown in Tables 4 and 5, although the migration rate in longitude in this study is lower, it still exhibits an onshore migration trend. We can consider the longitude and latitude migration trend obtained in this study as robust. The variations in migration rates between different studies can be attributed to the differences in the TC datasets used, the methods employed for trend analysis, and the variation in the definition of LMI across this study. These differences could potentially introduce variations across analyses. The longitudinal migration rate is lower and the latitudinal migration rate is moderate, indicating a significant northward trend compared to the coastal migration trend in the ECCO. However, it's worth noting that this study did not analyse the TC tracks in other TC datasets, which is a topic that warrants further investigation.

4.2. Landward extent of TC centers after landfall

The ocean affects the land through mass transport and transfer of energy, primarily manifesting as waves, tides, and even extreme weather events such as TCs (Gao et al., 2023). Therefore, the spatial-temporal variations of TC tracks are crucial in understanding their effect on land. We derived the westernmost boundaries reached by TC centers while maximum wind speed still exceeded 17.2 m/s , for TC tracks of Type 1 and Type 2 in each of the three historical periods (Fig. 8). 17.2 m/s is chosen as the threshold wind speed because this corresponds to the threshold for a severe weather alert in China. We observed that Type 1 primarily lands in the southern provinces of China, including Guangxi, Guangdong, and Fujian. Moreover, over time, the land area traversed by TC centers while those TCs still have maximum wind speed greater than 17.2 m/s after landfall for Type 1 is gradually expanding. Type 2, on the other hand, predominantly lands in the eastern provinces of China, including Jiangsu, Shanghai, and Zhejiang. Similar to Type 1, Type 2 also exhibits a trend of expanding land areas with wind speed exceeding 17.2 m/s over time. The proportion of Type 2

Table 4

The migration rate of LMI in longitude. Positive values of migration rate represent migration towards the coast (landward). CMA (China Meteorological Administration), IBTrACS (International Best Track Archive for Climate Stewardship), JTWC (Joint Typhoon Warning Center), and JMA (Japan Meteorological Agency).

Time period	Migration rate in longitude ($^\circ/\text{decade}$)	Datasets	Source
1979–2018	0.53	JMA	Li et al., 2022
1979–2018	0.61	CMA	Li et al., 2022
1979–2018	0.57	JTWC	Li et al., 2022
1982–2012	0.43	IBTrACS	Wang and Toumi, 2021
1979–2018	0.2	CMA	This study

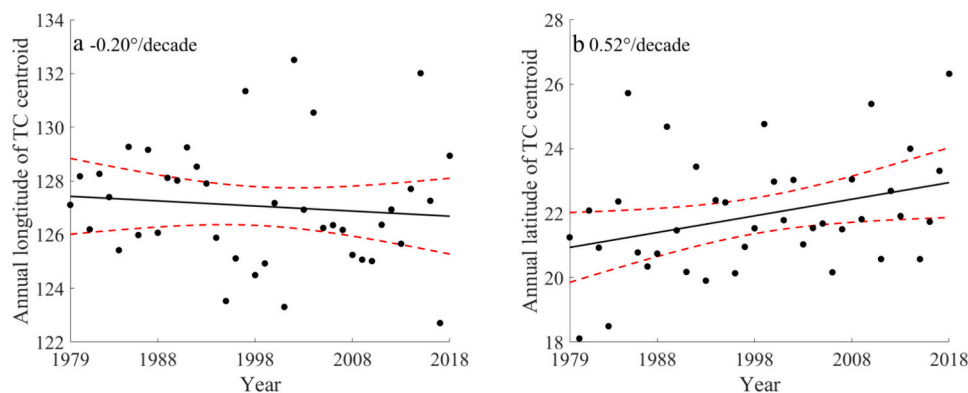


Fig. 7. The linear trend of annual mean longitude and latitude of TC centroid during 1979–2018. a is longitude, and b is latitude. The black solid line is the linear trend, and the red dashed line is the 95 % confidence interval. (For interpretation of the references to colour in this figure legend, the reader is referred to the web version of this article.) (For interpretation of the references to colour in this figure legend, the reader is referred to the web version of this article.) (For interpretation of the references to colour in this figure legend, the reader is referred to the web version of this article.)

Table 5

The migration rate of LMI in latitude. Positive values of migration rate represent poleward migration.

Time period	Migration rate in latitude (°/decade)	Datasets	Source
1979–2018	0.50	CMA	Meng et al., 2023
1979–2018	0.61	JTWC&CMA	Feng et al., 2021
1982–2012	0.47	IBTrACS	Moon et al., 2015
1982–2012	0.37	IBTrACS	Kossin et al., 2014
1979–2018	0.51	CMA	This study

TCs increases over time (Table 3), as discussed in section 4.1. Therefore, even though the overall number of TCs in the WNP is decreasing (Lee et al., 2020), the migration of these TC tracks could lead to more TCs impacting the eastern and northern regions of China. As described in section 3.3, the percentage of Type 1 decreases but the landfall percentage of Type 1 increases over time. This may be because the effect of Type 1 is more concentrated in southern China. Due to the northeastward movement of TC tracks, the percentage of Type 1 is decreasing and gradually shifting towards Type 2, which affects eastern China. This aligns with the results of Zhao et al. (2013). Additionally, the increasing landfall percentage of Type 1 can be attributed to the onshore migration trend of TC tracks (Wang and Toumi, 2021). In summary, the percentage of Type 1 decreases and the percentage of Type 2 increases, which means more TCs will strike the north and east parts of the ECCO. Landfall percentages of both Type 1 and 2 show increase (Table. 3), TCs affecting the ECCO and making landfall in the ECCO are gradually increasing in frequency, and the northern and eastern part of ECCO will face more TC disasters. The probability of TC effects on China's eastern and northern regions is increasing, and the boundaries reached by the TC center are increasing westward. This provides planning suggestions for disaster reduction in northern cities to enhance their response capabilities to future extreme events. Additionally, it offers reference points for

defining research boundaries when planning coastal zones.

4.3. Factors affecting TC tracks

The migration of the TC tracks is related to environmental conditions, especially the mesoscale steering flow, VWS, and the SST (Mei et al., 2015; Camargo and Wing, 2021; Wang and Toumi, 2021). The steering flow can lead the movement of TCs. A high VWS environment is known to be one of the main reasons for the failure of TC development and for the weakening of TCs (Gray, 1968). Similarly to VWS, the SST in the lower latitude western North Pacific (LLWNP, 5°–15°N, 130°–180°E) energizes TC generation (Mei et al., 2015; Mei and Xie, 2016) and warming SST can lead to meridional expansion of the tropical region (Sharmila and Walsh, 2018). This could provide a theoretical upper limit of the energy for the northward movement of TCs. Therefore, in this section, we will explain the changes in TC tracks in terms of changes in these three environmental conditions. Steering flow is defined as mid-tropospheric (500 hPa) wind fields (Wang et al., 2022). It aligns with the pressure-weighted deep-layer wind field between 300 and 850 hPa (Aryal et al., 2018). VWS is calculated by the wind field between 200 and 850 hPa (Zehr, 2003).

From section 3.3, we learned that the active months for TC activity in the ECCO are from May to October. Therefore, we derive the mean steering flow, VWS, and SST in the three periods from May to October and calculate the spatial difference of steering flow, VWS, and SST as shown in Fig. 9.

From Fig. 9a, during the second period, the westward steering flow strengthened between 20°–40°N compared to the first period. This could lead to eastward migration of TC tracks. The difference in mean tracks between p2c1 and p2c2 is significantly greater than between p1c1 and p1c2. This difference could be related to a cyclonic northeastward steering flow change on the west side of Taiwan. This might cause some TCs whose tracks are located between Type 1 and Type 2 moving

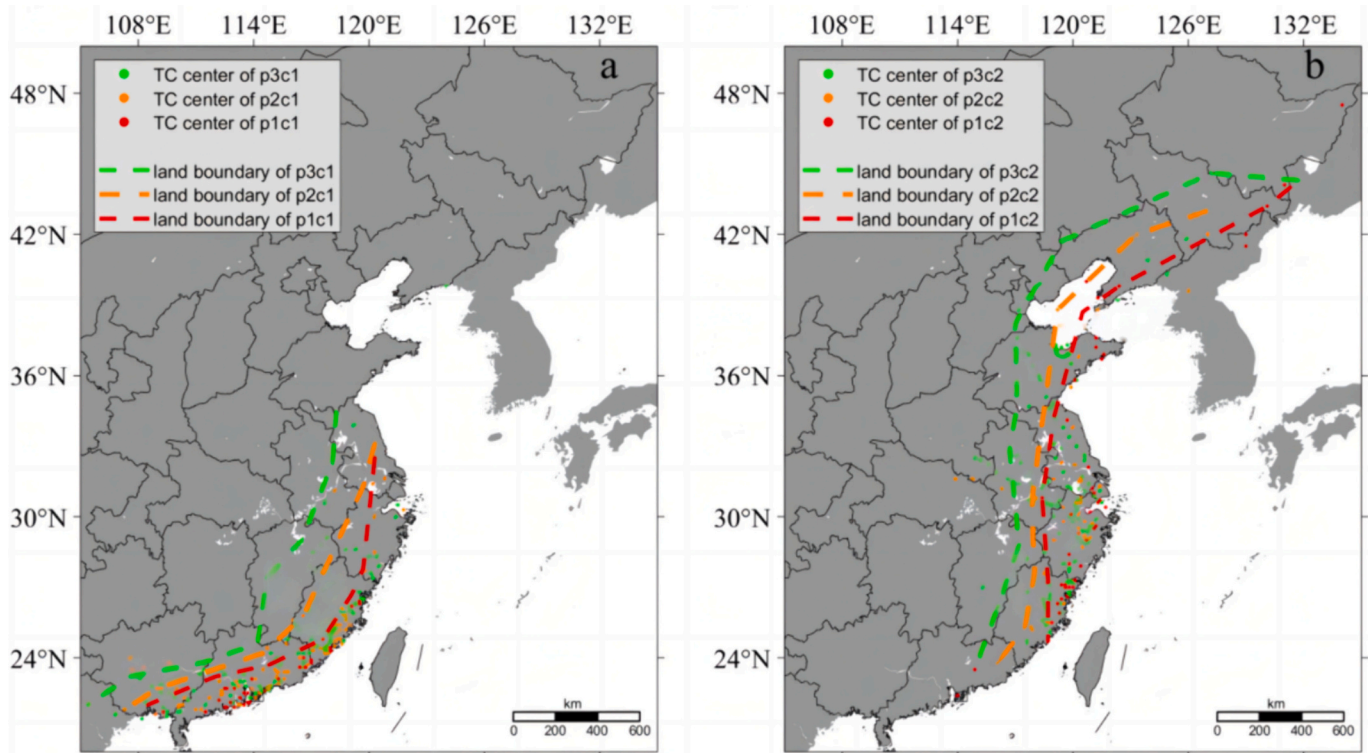


Fig. 8. Boundaries reached by TC centers after landfall with maximum wind speed exceeding 17.2 m/s. Panel a represents the land range of Type 1 during the three periods, while Panel b shows the land range of Type 2 during the three periods. Type 3, due to their limited number, was not analyzed in this study. The points indicate the TC centers and the dashed lines represent the TC land boundaries.

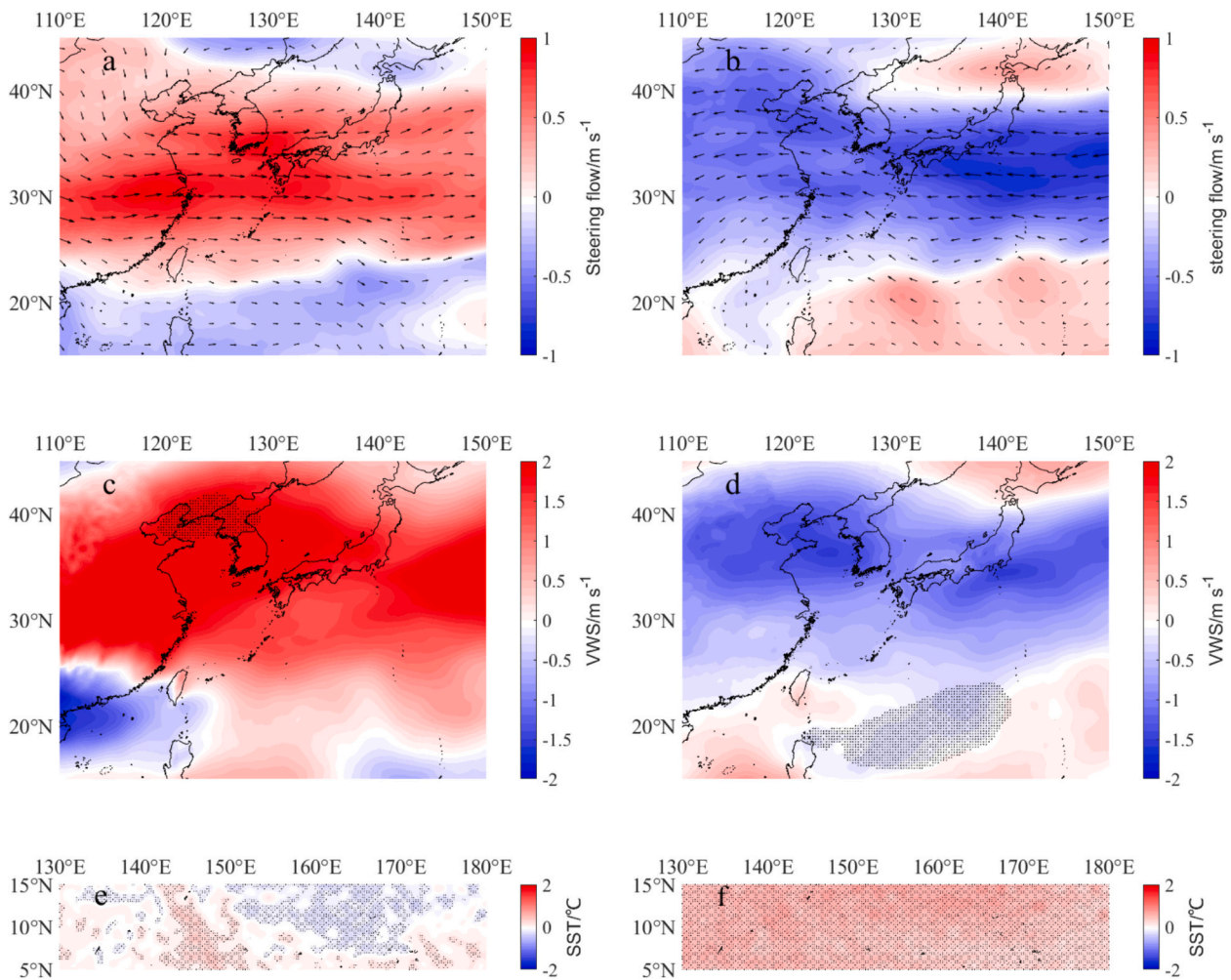


Fig. 9. Spatial difference of steering flow, VWS, and SST from May to October. a, b are the differences in steering flow; c, d are the differences in VWS; e, f are the differences in SST in the LLWNP. The left figures are the difference between the first (1949–1967) and second (1968–1993) periods, and the right figures are the difference between the second (1968–1993) and third (1994–2022) periods. The black dots indicate where the difference is significant at a confidence level of 95 %.

northeastward, making their tracks similar to Type 2. Therefore, the distinctions between Type 1 and Type 2 in the second period in Section 3.2.2 become more pronounced compared to the first period. However, the VWS in this region strengthens (Fig. 9c), which suppresses the development of TCs. Therefore, the mean TC lifespan during the second period is significantly shorter than in the first period, as shown in section 3.3. Meanwhile, during the second period, the SST in LLWNP doesn't show significant changes relative to the first period. There is warming in the west but cooling in the east (Fig. 9e). Under the background of the combination of stronger VWS and relatively stable SST, the TCs did not gain much energy during this period. Therefore, the TC mean centroid during the second period exhibits only minor northeastward movement compared to the first period. In contrast, during the third period, the westward steering flow weakened (Fig. 9b). Additionally, there is a northwestward steering flow change near Taiwan, causing TC tracks to shift further towards the northwest. During the third period, the VWS decreased in the northern part of Taiwan (Fig. 9d), compared to the second period. This relative reduction in VWS provides a more favorable environment for the northward movement and development of TCs. However, the VWS in the south of Taiwan increased. This might lead to a decrease in the proportion of p3c1 and an increase in the proportion of p3c2 as described in section 3.3 (Table 3). Simultaneously, in the third period, the SST increased significantly compared to the second period (Fig. 9f). As a result, the theoretical upper limit of energy that TCs can gain while moving towards higher latitudes keeps rising. The combined

effect of these environmental conditions contributed to the more pronounced trend of TC tracks shifting both towards the coast and northward during the third period.

Although the migration of TC tracks in the ECCO has closely related to the steering flow, VWS and SST, the phase of Pacific Decadal Oscillation (PDO), El Niño-Southern Oscillation (ENSO), vorticity, relative humidity and other meteorological conditions also can influence TC activity (Mei et al., 2015; Wang et al., 2019; Zhao et al., 2020; Wang et al., 2022; Meng et al., 2023). This study has not analyzed other meteorological conditions. Investigating these factors could be a priority for future research on TCs within different clusters.

5. Conclusions

Based on the TC position, shape, and intensity information, three typical types of TC tracks in the ECCO since 1949 are derived. The clustering analysis offers an initial insight into the traits of TC tracks within each cluster. This study is a systematic approach to research the effect of representative TCs in a specific region by quantifying the magnitude of poleward and landward track migration. This is also of importance for the study of the regularity of TC changes in other regions of the world that are significantly affected by TCs. The main conclusions are as follows:

- Period 3 (1994–2022) represents a significant phase during which TC tracks underwent substantial migration. The mean centroid of the TCs affecting the ECCO shifted westward by 0.66° in longitude and northward by 1.26° in latitude. This migration trend is closely linked to mesoscale steering flow, VWS, and SST. The combination of weakening westward steering flow, reduced VWS, and warmer SST may have facilitated the northward and onshore development of tropical cyclones during Period 3.
- There are three typical types of TC tracks in the ECCO region. Type 1 is a northwestward track, Type 2 is a northwest to northeast-turning track, and Type 3 is a northwest to northeast-turning offshore track. Type 1 primarily makes landfall in southern China, whereas Type 2 predominantly affects eastern China. Furthermore, the percentage of Type 1 decreases but the landfall percentage of Type 1 increases over time. The percentage of Type 2 is on the rise, and the affected land boundary is shifting westward.
- TC lifespans range from 2 to 17 days, with the majority between 6 and 12 days. We categorize the active periods of the three typical types into three seasons: pre-peak, peak, and post-peak. For Type 1, the three seasons are April to June, July to September, and October to December, respectively. For Type 2, the seasons are May to June, July to September, and October. Due to the smaller number of Type 3 TCs, Type 3 is categorized into seasons consistent with Type 2 in this study.
- The probability of TCs affecting eastern and northern China is increasing due to the latitudinal and longitudinal migration of TC tracks. Regional planning for disaster prevention and mitigation can be informed by the spatial-temporal distribution of TC tracks.

This study uses one TC dataset (The CMA Dataset of TC Tracks) only to analyse the change of TC tracks, but there are also other meteorological conditions that can influence this. Analyzing the variations and disparities in TC tracks by integrating different TC datasets and considering more meteorological parameters will be a crucial aspect of our future research endeavors.

CRedit authorship contribution statement

Chaoran Xu: Writing – original draft, Software, Methodology, Data curation. **Jianjun Jia:** Writing – review & editing, Project administration, Data curation, Conceptualization. **Jeremy D. Bricker:** Writing – review & editing, Project administration, Data curation. **Ya Ping Wang:** Writing – review & editing.

Declaration of competing interest

We declare that we do not have any commercial or associative interest that represents a conflict of interest in connection with the work submitted.

Data availability

Data will be made available on request.

Acknowledgment

This study was supported by the National Natural Science Foundation of China (No. 41876092, No. 42276050, U2240220); the US National Science Foundation (grant Nos. 2228486 and 2228485) and the China Scholarship Council (No. 202206140090).

References

Aryal, Y.N., Villarini, G., Wei, Zhang, et al., 2018. Long term changes in flooding and heavy rainfall associated with North Atlantic tropical cyclones: Roles of the North Atlantic Oscillation and El Niño-Southern Oscillation. *J. Hydrol.* 559, 698–710.

- Bangladesh, 2020. World's Deadliest Tropical Cyclone Was 50 Years Ago. World Meteorological Organization.
- Camargo, S.J., Wing, A.A., 2021. Increased tropical cyclone risk to coasts. *Science* 371 (6528), 458–459.
- Camargo, S.J., Robertson, A.W., Gaffney, S.J., et al., 2007. Cluster analysis of typhoon tracks. Part i: general properties. *J. Clim.* 20 (14), 3635–3653.
- Chang, Lei, Yu, Jinhua, 2017. Analysis of tropical cyclone motion velocity anomalies over the western North Pacific and their forecast. *Trans. Atmos. Sci. (in Chinese)* 01 (1), 71–80.
- Colbert, A.J., Soden, B.J., 2012. Climatological variations in North Atlantic tropical cyclone tracks. *J. Clim.* 25 (2), 657–673.
- Emanuel, K.A., 1986. An air-sea interaction theory for tropical cyclones. Part I: steady-state maintenance. *J. Atmos. Sci.* 43 (6), 585–604.
- Emanuel, K.A., 1999. Thermodynamic control of hurricane intensity. *Nature* 401 (6754), 665–669.
- Emanuel, K., 2003. Tropical cyclones. *Annu. Rev. Earth Planet. Sci.* 31 (1), 75–104.
- Feng, Jingxian, Lu, Xiaoqin, Yu, Hui, et al., 2014. An overview of the China Meteorological Administration tropical cyclone database. *J. Atmos. Ocean. Technol.* 31 (2), 287–301.
- Feng, Xiangbo, Klingaman, N.P., Hodges, K.I., 2021. Poleward migration of western North Pacific tropical cyclones related to changes in cyclone seasonality. *Nat. Commun.* 12 (1), 6210.
- Gao, Shu, Jia, Jianjun, Yu, Qian, 2023. Theoretical framework for coastal accretion-erosion analysis: material budgeting, profile morphology, shoreline change. *Mar. Geol. Quat. Geol. (in Chinese)* 2, 1–17.
- Gray, W.M., 1968. Global view of the origin of tropical disturbances and storms. *Mon. Weather Rev.* 96 (10), 669–700.
- Hawkes, A.D., Horton, B.P., 2012. Sedimentary record of storm deposits from Hurricane Ike, Galveston and San Luis Islands, Texas. *Geomorphology* 171, 180–189.
- Hersbach, H., Bell, B., Berrisford, P., et al., 2023a. ERA5 monthly averaged data on pressure levels from 1940 to present. In: Copernicus Climate Change Service (C3S) Climate Data Store (CDS) (Accessed on DD-MMM-YYYY).
- Hersbach, H., Bell, B., Berrisford, P., et al., 2023b. ERA5 monthly averaged data on single levels from 1940 to present. In: Copernicus Climate Change Service (C3S) Climate Data Store (CDS) (Accessed on DD-MMM-YYYY).
- Hu, Yuyi, Shao, Weizeng, Wei, Yongliang, et al., 2020. Analysis of typhoon-induced waves along typhoon tracks in the Western North Pacific Ocean, 1998–2017. *J. Mar. Sci. Eng.* 8 (7).
- Kamahori, H., Yamazaki, N., Mannoji, N., et al., 2006. Variability in intense tropical cyclone days in the Western North Pacific. *Sola* 2, 104–107.
- Kaufman, L., Rousseeuw, P.J., 1990. *Finding Groups in Data: An Introduction to Cluster Analysis*. Wiley, New York, p. 342.
- Kim, H.S., Kim, J.H., Ho, C.H., et al., 2011. Pattern classification of typhoon tracks using the fuzzy c-means clustering method. *J. Clim.* 24 (2), 488–508.
- Kossin, J.P., Emanuel, K.A., Vecchi, G.A., 2014. The poleward migration of the location of tropical cyclone maximum intensity. *Nature* 509 (7500), 349–352.
- Kossin, J.P., Emanuel, K.A., Camargo, S.J., 2016. Past and projected changes in Western North Pacific tropical cyclone exposure. *J. Clim.* 29 (16), 5725–5739.
- Lee, Tszy-Cheung, Knutson, Thomas R., Nakaegawa, Toshiyuki, et al., 2020. Third assessment on impacts of climate change on tropical cyclones in the Typhoon Committee Region – part I: observed changes, detection and attribution. *Trop. Cyclone Res. Rev.* 9 (1), 1–22.
- Li, WeiBiao, Du, QinBo, Chen, ShuMin, 2010. Climatological relationships among the tropical cyclone frequency, duration, intensity and activity regions over the Western Pacific. *Chin. Sci. Bull.* 55 (33), 3818–3824.
- Li, Guangxin, Li, Qinglan, Xu, Yinglong, et al., 2022. Changes of tropical cyclones landfalling in China from 1979 to 2018. *J. Geophys. Res. Atmos.* 127 (16), e2022JD036701.
- Liu, Kam-Biu, Shen, Caiming, Louie, Kin-Sheun, 2001. A 1,000-year history of typhoon landfalls in Guangdong, Southern China, reconstructed from Chinese historical documentary records. *Ann. Assoc. Am. Geogr.* 91 (3), 453–464.
- Lu, Xiaoqin, Yu, Hui, Ying, Ming, et al., 2021. Western North Pacific tropical cyclone database created by the China Meteorological Administration. *Adv. Atmos. Sci.* 38 (4), 690–699.
- Luo, Xi, Yang, Lei, Chen, Sheng, et al., 2022. The decadal variation of eastward-moving tropical cyclones in the South China Sea during 1980–2020. *Geophys. Res. Lett.* 49 (5), e2021GL096640.
- Mei, Wei, Xie, Shang-Ping, 2016. Intensification of landfalling typhoons over the Northwest Pacific since the late 1970s. *Nat. Geosci.* 9 (10), 753–757.
- Mei, Wei, Xie, Shang-Ping, Primeau, F., et al., 2015. Northwestern Pacific typhoon intensity controlled by changes in ocean temperatures. *Sci. Adv.* 1 (4), e1500014.
- Meng, Wenjian, Zhang, Kewei, Liu, Haijiang, 2023. The poleward migration of tropical cyclolysis in the Western North Pacific. *J. Clim.* 36 (20), 7143–7155.
- Ming, A., Rowell, I., Lewin, S., et al., 2021. Key Messages from the IPCC AR6 Climate Science Report. Cambridge Open Engage.
- Moon, L.J., Kim, S.H., Klotzbach, P., et al., 2015. Roles of interbasin frequency changes in the poleward shifts of the maximum intensity location of tropical cyclones. *Environ. Res. Lett.* 10 (10), 104004.
- Muis, S., Verlaan, M., Winsemius, H.C., et al., 2016. A global reanalysis of storm surges and extreme sea levels. *Nat. Commun.* 7 (1), 11969.
- Nakamura, J., Lall, U., Kushnir, Y., et al., 2009. Classifying North Atlantic tropical cyclone tracks by mass moments. *J. Clim.* 22 (20), 5481–5494.
- Nakamura, J., Camargo, S.J., Sobel, A.H., et al., 2017. Western North Pacific tropical cyclone model tracks in present and future climates. *J. Geophys. Res. Atmos.* 122 (18), 9721–9744.

- Nakamura, J., Lall, U., Kushnir, Y., et al., 2021. Early season hurricane risk assessment: climate-conditioned HITS simulation of North Atlantic tropical storm tracks. *J. Appl. Meteorol. Climatol.* 60 (4), 559–575.
- Paliwal, M., Patwardhan, A., 2013. Identification of clusters in tropical cyclone tracks of North Indian Ocean. *Nat. Hazards* 68, 645–656.
- Qian, Qifeng, Jia, XiaoJing, Lin, Yanluan, 2022. Reduced tropical cyclone genesis in the future as predicted by a machine learning model. *Earth's Future* 10 (2).
- Schuerch, M., Dolch, T., Reise, K., et al., 2014. Unravelling interactions between salt marsh evolution and sedimentary processes in the Wadden Sea (southeastern North Sea). *Prog. Phys. Geogr. Earth Environ.* 38 (6), 691–715.
- Sharmila, S., Walsh, K.J.E., 2018. Recent poleward shift of tropical cyclone formation linked to Hadley cell expansion. *Nat. Clim. Chang.* 8 (8), 730–736.
- Shen, Yixuan, Sun, Yuan, Zhong, Zhong, et al., 2018. Sensitivity experiments on the poleward shift of tropical cyclones over the Western North Pacific under warming ocean conditions. *J. Meteorol. Res.* 32 (4), 560–570.
- Song, Wanjiao, Tang, Shihao, Wang, Xin, 2018. Relationship between Pacific Ocean warming and tropical cyclone activity over the western North Pacific. *Stoch. Env. Res. Risk A.* 33 (1), 31–45.
- Ting, M., Kossin, J.P., Camargo, S.J., et al., 2019. Past and future hurricane intensity change along the U.S. East Coast. *Sci. Rep.* 9 (1), 7795.
- Wang, Bo, Song, Yuanming, 2011. Study on the difference of amorphous substances of coal ashes. *Adv. Mater. Res.* 287, 1189–1192.
- Wang, Shuai, Toumi, R., 2021. Recent migration of tropical cyclones toward coasts. *Science* 371 (6528), 514–517.
- Wang, Tianju, Zhong, Zhong, Sun, Yuan, et al., 2019. Impacts of tropical cyclones on the meridional movement of the western Pacific subtropical high. *Atmos. Sci. Lett.* 20 (5).
- Wang, Ke, Yang, Yongsheng, Reniers, Genserik, et al., 2021. A study into the spatiotemporal distribution of typhoon storm surge disasters in China. *Nat. Hazards* 108 (1), 1237–1256.
- Wang, Licheng, Gu, Xihui, Gulakhmadov, A., et al., 2022. An analysis of translation distance of tropical cyclones over the Western North Pacific. *J. Clim.* 35 (23), 7643–7660.
- Wu, Man-Chi, Yeung, Kai-Hing, Chang, Wen-Lam, 2006. Trends in western North Pacific tropical cyclone intensity. *EOS Trans. Am. Geophys. Union* 87 (48), 537–538.
- Xu, Sudong, Huang, Wenrui, 2011. Estimating extreme water levels with long-term data by GEV distribution at Wusong station near Shanghai city in Yangtze Estuary. *Ocean Eng.* 38 (2–3), 468–478.
- Xu, Chaoran, Yang, Yang, Zhang, Fan, et al., 2022. Spatial-temporal distribution of tropical cyclone activity on the eastern sea area of China since the late 1940s. *Estuar. Coast. Shelf Sci.* 277.
- Yang, Shuo, Liu, Xin, Liu, Qiang, 2016. A storm surge projection and disaster risk assessment model for China coastal areas. *Nat. Hazards* 84 (1), 649–667.
- Yin, Yafeng, Yong, Yangyang, Qi, Shandong, et al., 2023. Cluster analyses of tropical cyclones with genesis in the South China Sea based on K-means method. *Asia-Pac. J. Atmos. Sci.* 59 (4), 433–446.
- Yu, Jinhua, Zheng, Yingqin, Wu, Qishu, et al., 2016. K-means clustering for classification of the northwestern Pacific tropical cyclone tracks. *J. Trop. Meteorol.* 22 (2), 127–135.
- Yumoto, M., Matsuura, T., Iizuka, S., 2003. Interdecadal variability of tropical cyclone frequency over the Western North Pacific in a high-resolution atmosphere-ocean coupled GCM. *J. Meteorol. Soc. Jpn.* 81 (5), 1069–1086.
- Zehr, R.M., 2003. Environmental vertical wind shear with hurricane Bertha (1996). *Weather Forecast.* 18 (2), 345–356.
- Zhang, Qianying, Zhong, Shaobo, Huang, Quanyi, 2015. Classification of tropical cyclone tracks striking Guangdong from 1949–2013 based on Fuzzy c-means (in Chinese). *J. Catastrophol.* 30 (4), 187–193.
- Zhao, Haikun, Wu, Liguang, Wang, Rui Fang, 2013. Decadal variations of intense tropical cyclones over the western North Pacific during 1948–2010. *Adv. Atmos. Sci.* 31 (1), 57–65.
- Zhao, Haikun, Klotzbach, P.J., Chen, Shaohua, 2020. Dominant influence of ENSO-like and global sea surface temperature patterns on changes in prevailing boreal summer tropical cyclone tracks over the Western North Pacific. *J. Clim.* 33 (22), 9551–9565.
- Zheng, Yingqin, Yu, Jinhua, Wu, Qishu, et al., 2015. K-means clustering method for classification of the Northwestern Pacific tropical cyclone tracks. *J. Trop. Meteorol. (in Chinese)* 29 (4), 607–615.